Evaluation of the Corrosion Resistance of $Fe_{40}Al_{60}$ Intermetallics in Molten Carbonate (Li+K)

G. Pedroza[1,3], A.Martinez-Villafane[1], M.A. Espinoza-Medina[2], M.A.Rivera[3] and P.J. Sebastian[4,*]

[1]Centro de Investigación en Materiales Avanzados, División de Ciencia e Ingeniería Ambiental, Miguel de Cervantes 120, Complejo industrial Chihuahua, 31109 Chihuahua, México
[2]Facultad de Ingeniería Mecánica, UMSNH, Santiago Tapia 403 Col. Centro, C.P. 58000 Morelia, Michoacán, Mexico
[3]Universidad Politecnica del Estado de Guerrero, Carr. Taxco-Iguala s/n, Col. Arroyo, Taxco de Alarcon, Guerrero, México
[4]Centro de Investigación en Energía-UNAM, 62580, Temixco, Morelos, México

Abstract: *Alloys of the intermetallic material based on $Fe_{40}Al_{60}$ and the alloys formed with addition of Ag constitute a new alternative to improve the problems of corrosion resistance and electrical conductivity. The electrochemical characterization was employed to evaluate the corrosion resistance of the materials for being used as bipolar plates in molten carbonate fuel cells (MCFC). These characterizations were done under similar conditions as the working environment of the molten carbonate fuel cell (MCFC). The working environment of the standard molten carbonate fuel cell was simulated by the use of molten salts of 62 mol.% Li_2CO_3 and 38 mol.% K_2CO_3 at the temperature of 650 ºC. Alloys included $Fe_{40}Al_{60}$ with additions of 1, 3 and 5 weight % of Ag. The results obtained indicate that this material is promising for its use as bipolar plates in MCFC.*

1. INTRODUCTION

The molten carbonate fuel cell (MCFC) is believed to be one of the most promising new energy conversion devices that convert chemical energy into electrical energy. It is a highly efficient and environmentally clean source of power. Nevertheless, it has a limiting aspect in the current collectors due to the corrosion of the metallic parts. The molten carbonate fuel cells (MCFCs) can be considered as a new and alternative power source, promising due to its low environmental emission and high efficiency. They can convert the chemical energy of a reaction into electrical energy with no intermediate conversion of heat into mechanical energy [1].

For successful market-entry and competitiveness of MCFC systems, reduction of costs, improvement of reliability and endurance are required. A limiting aspect for reaching the goal of 40,000 hrs of lifetime is the corrosion of active areas of the metallic parts of MCFC, especially in the anodic region. In fact, the operating con-

ditions on the anode side are more severe and the material must resist a reducing and carburizing environment at high temperature and in presence of molten carbonates that partially impregnate the anode [2].

Conventional molten carbonate fuel cells (MCFC) operate at 650 ◦C and consist of several cells made of a porous, lithiated NiO cathode, a molten $(Li,K)_2CO_3$ electrolyte in a $LiAlO_2$ ceramic matrix and a porous Ni anode [3,4]. Austenitic stainless steels such as 310S, 316 or 316L are typically used for cathode current collectors and bipolar separator plates [5–8]. Corrosion of austenitic stainless steels (SS) used as bipolar plates and cell-housing materials in molten carbonate fuel cells (MCFC) still represent a serious technological item that may adversely affect the useful lifetime of the fuel cell. In particular, the bipolar plate suffers from the major corrosion problems since this component is in contact with three different environments: the cathode area (oxidizing gas environment), the anode area (reducing gas environment) and the so-called 'wet-seal' region where the plate is covered with a continuous and thick film of the corrosive carbonate electrolyte and the local gas composition may fluctuate considerably giving rise to

*To whom correspondence should be addressed: Email: sjp@cie.unam.mx
Phone:

insidious micro-galvanic corrosion cells [9].

FeAl type intermetallics are widely used for their high temperature oxidation resistance due to their ability to develop an Al_2O_3 protective layer, which also provides corrosion resistance in molten salts [10-11]. However, one of the main drawbacks for these aluminides is their poor ductility. Salazar et al. [12] found that by alloying with either Li or Ni results in the improvement of their ductility as measured in their compressive ductility, and this improvement was increased if the specimens were annealed at 400 °C during 120 hrs. The aim of this work is thus to evaluate the effect of the additions of small quantities of Ag followed by a heat treatment on the corrosion resistance of Fe40Al60 in molten $(Li,K)_2CO_3$ at 650 °C and compare them with that for 316L type stainless steel, a commonly used material in bipolar plates in MCFC.

2. EXPERIMENTAL PROCEDURE

It should be recalled that corrosion of bipolar plate depends strongly on the contact area with the carbonate melt containing the dissolved gaseous oxidant. In the wet-seal area, the plate is covered with a thick film of carbonate melt, so it mostly resembles a fully immersed piece of corroding sample in the melt. Conversely, the areas of the plate in contact with the electrodes can be described as composed of both dry and electrolyte-covered areas. Therefore, dip tests have been performed in a fully immersed condition to simulate the wet-seal area condition of the bipolar plate.

The specimens were prepared as square parallelepipeds having a size of 10 x10 x3 mm for polarization curves. These specimens for electro-chemical techniques were the working electrodes, to which an 80 wt.% Cr–20Ni wire was spot-welded. This wire was used as electrical connection between the working electrode and the potentiostat. The specimens were ground to 1200 grade emery paper, washed in distilled water, degreased with acetone and dried under an air stream. For electrochemical measurements, the reference electrode and counter electrode were 5 mm diameter and 300 mm long platinum wires. In previous reported studies, the platinum electrode was tested to assess its stability as a reference electrode under the experimental conditions considered in the present work [13].

Electrochemical tests were done using a Solartron 1260 potentiostat, controlled by a personal computer. In the electrochemical measurements, some areas of the samples remained un-immersed in the melt. The electrochemical measurements were performed at 650°C in the eutectic Li/K carbonate melt (62 mol % Li_2CO_3 + 38 mol % K_2CO_3), during 120 hrs.

The FeAl alloys, with chemical compositions as shown in the table 1, were obtained under conventional gravity casting techniques with pure Fe, Al and Ag. Each sample specimen was subjected to mechanical polishing to reveal the microstructure of the alloys.

Table 1. The chemical composition of the alloys used.

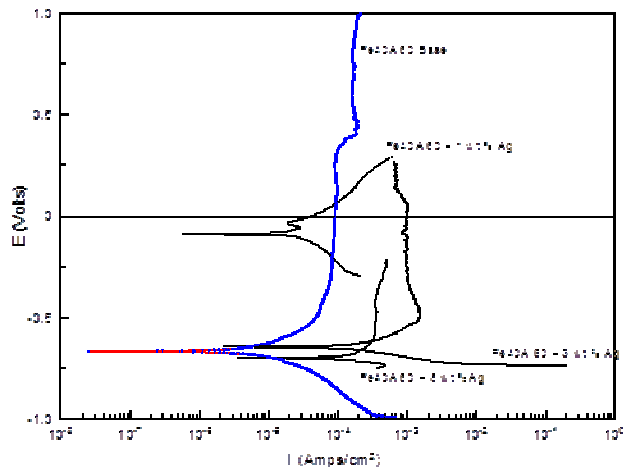| Alloy	Chemical composition
$Fe_{40}Al_{60}$ (base alloy)	Al-60 wt.%, Fe-40 wt %
$Fe_{40}Al_{60}$ + 1 % Ag	$Fe_{40}Al_{60}$ +1 at. % of Ag
$Fe_{40}Al_{60}$+ 3 % Ag	$Fe_{40}Al_{60}$ + 3 at. % of Ag
$Fe_{40}Al_{60}$ + 5 % Ag	$Fe_{40}Al_{60}$ + 5 at. % of Ag

Figure 1. The potentiodynamic polarization curves for the base alloy $Fe_{40}Al_{60}$ along with the inter-metallics with 1, 3 and 5 wt. % of Ag.
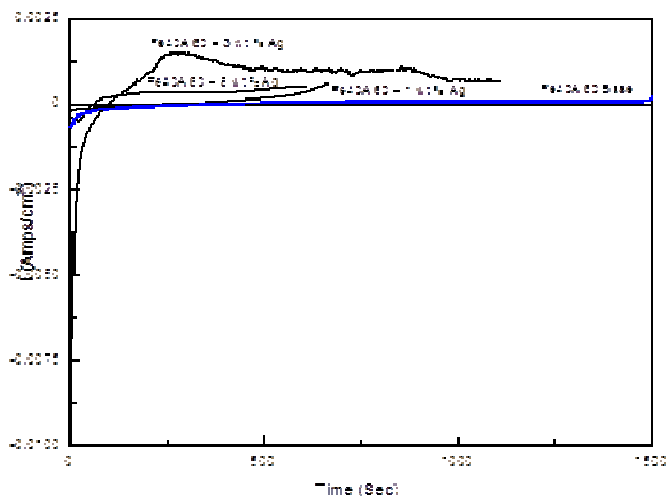

Figure 2. L_{PR} curves for the base alloy $Fe_{40}Al_{60}$ along with the inter-metallics with 1, 3 and 5 wt. % of Ag, using conditions similar to that of a molten carbonate fuel cell.

3. RESULTS AND DISCUSSION

The materials considered in this work were analyzed to determine their functional characteristics considering their use as bipolar plates in molten carbonate fuel cells. The electrochemical characterization was performed at 650°C in Li/K molten salt electrolyte. The melting point of the salt (62 mol % Li_2CO_3 + 38 mol % K_2CO_3) is close to 500°C, depending on the environmental conditions. The experiment simulated the conditions of operation of the current collectors in MCFC.

The electrochemical characteristics of the base material $Fe_{40}Al_{60}$ and the intermetallic compounds of $Fe_{40}Al_{60}$ with 1,3 and 5 at. % of Ag were analyzed by the potentiodynamic technique. The polarization curves for the base material and the three intermetallic alloys are shown in figures 1-3.

Evaluation of the Corrosion Resistance of $Fe_{40}Al_{60}$ Intermetallics in Molten Carbonate (Li+K)
/ J. New Mat. Electrochem. Systems

23

Figure 1 shows the potentiodynamic polarization curves for the base alloy $Fe_{40}Al_{60}$ along with the inter-metallics with 1, 3 and 5 wt. % of Ag. The electrochemical kinetic parameters for the base alloy and the intermetallic materials were determined. For the base alloy, the corrosion current density (I_{corr}) during anodic polarization was determined as 1.58×10^{-5} amp/cm^2 and the open circuit potential (E_0) as -0666 volts. The kinetic parameters for the intermetallic alloys were determined and the values are as follows:

$Fe_{40}Al_{60}$ + 1 wt. % Ag

Anodic polarization = -1648.6 mV, cathodic polarization = -413.27mV, the corrosion current density (I_{corr}) = 8.1572×10^{-5} amp/cm^2 and the open circuit potential (E_0) = -0.088312 Volts.

$Fe_{40}Al_{60}$ + 3 wt. % Ag

Anodic polarization = -194.93mV, cathodic polarization = -84.414 mV, I_{corr} = 3.0638×10^{-4} amp/cm^2 and the open circuit potential (E_0) = -0.64448 Volts.

$Fe_{40}Al_{60}$ + 5 wt. % Ag

Anodic polarization = -1843.27 mV, the cathodic polarization = -119.07 mV, the corrosion current density (I_{corr}) = 3.9367×10^{-4} amp/cm^2 and the open circuit potential (E_0) = -0.70106 Volts.

The above results are summarized in table 2 for comparison. One can see that in the case of the intermetallic materials with 1, 3 and 5 wt. % of Ag, the values of the corrosion current densities are more positive than that of the base material and in the case of the material with 3% Ag the anodic polarization is lower than that for the base material. For the other compositions the anodic polarizations are higher than that of the base material.

Wang et al. [14] established that for the material to be used as bipolar plate in molten carbonate fuel cell, the I_{corr} may be of the order of 10^{-6} Amp/cm^2 or lower at a corrosion potential of the order of -0.01V SCE, which is recommended as a starting point. From the analysis of the polarization curves for the base material and the inter-metallics with 1, 3 and 5 wt. % of Ag, one could see that the corrosion current is between 10^{-4} and 10^{-5} A/cm^2, an order of magnitude higher than the reference value recommended by Wang et al., although in the case of aluminum the corresponding value is 10 times higher. This difference in corrosion behavior between the base material and the inter-metallics can be explained by what has been proposed by Sankara Narayanan [15], who established that for deposits of ternary alloys with variation of the metal composition significantly influences the characteristic properties of the coatings. Mesa and coworkers [16] obtained similar results for 304 stainless steel covered with Li and tested in sulfuric acid and for 316 stainless steel tested in 0.01M HCl + 0.01M Na_2SO_4 electrolyte.

The inter-metallics maintain a corrosion potential value in the range of 250 mV – 700 mV and have corrosion currents in the range 10^{-4} A/cm^2 - 10^{-5} A/cm^2, which can be considered as acceptable values for their performance as corrosion resistant materials in
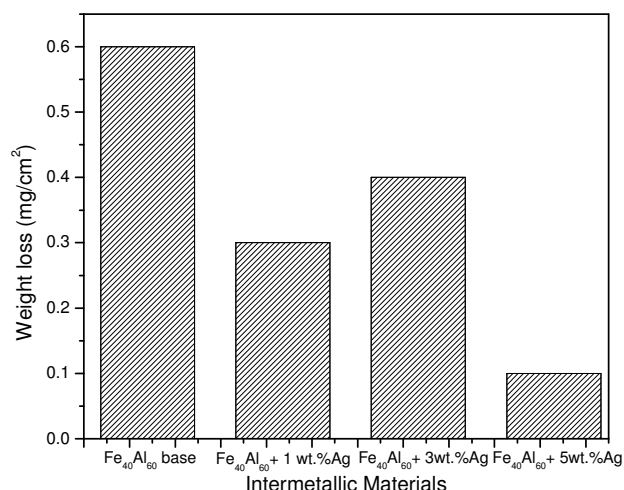

Figure 3. The Effect of weight loss for the base alloy $Fe_{40}Al_{60}$ along with the inter-metallics with 1, 3 and 5 wt. % of Ag.

molten carbonate fuel cells. Since a large amount of Ag is deposited in the intermetallic materials, their electrical conductivity increases and hence are vulnerable to corrosion. These curves (polarization) are important because one obtains from those the anodic (B_a) and the cathodic Tafel slopes (B_c), which can be used to calculate the corrosion current density (I_{corr}) and corrosion rate in terms of the linear polarization resistance (L_{PR}) obtained from the Stern –Geary equation.

$I_{corr} = B/L_{PR}$

where

$B = B_a.B_c / 2.303(B_a+B_c)$, B_a and B_c are the Tafel slopes (obtained from the polarization curves).

The I_{corr} values obtained by the L_{PR} test are shown in figure 2 for the base material $Fe_{40}Al_{60}$ and for the alloys with Ag. It can be seen that in general the inter-metallic alloys behave similar to the base material $Fe_{40}Al_{60}$, but as time went on had a slight increase in I_{corr} values except for $Fe_{40}Al_{60}$ + 3 % Ag which maintained a constant small corrosion current with time. The $Fe_{40}Al_{60}$ + 3 % Ag which presented a small decrease in the corrosion current and a more stable behavior compared to the other inter-metallics. The base material $Fe_{40}Al_{60}$ began with a normal corrosion, as time passed the I_{corr} tends to stabilize and has a smaller fluctuation in corrosion current compared to the other three materials.

The weight loss tests were conducted with substrates of 5 x 5 x 2 mm sizes. The samples were immersed in molten salt of composition, 62 mol % of Li_2CO_3 + 38 mol % of K_2CO_3 at a temperature of

Table 2. The anodic current densities, cathodic corrosion and the potential for each of the samples studied.

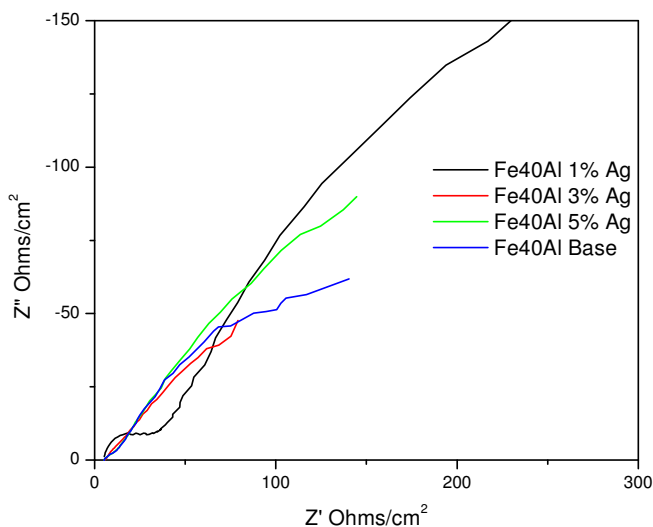|	Anodic polarization (mV)	Cathodic polarization (mV)	Corrosion current (amp/cm^2)	Open circuit potential (V)
$Fe_{40}Al_{60}$	-323.01	-212.760	1.5800E-5	-0.66600
$Fe_{40}Al_{60}$ + 1% Ag	-1648.60	-413.270	8.5172E-5	-0.088312
$Fe_{40}Al_{60}$ + 3% Ag	-194.93	-84.414	3.0638E-04	-0.64448
$Fe_{40}Al_{60}$ + 5% Ag	-1843.27	-119.07	3.9367E-04	-0.70106

Figure 4. The Nyquist plots for the corrosion of the base alloy $Fe_{40}Al_{60}$ along with the inter-metallics with 1, 3 and 5 wt. % of Ag in the molten salt (62 mol % Li_2CO_3 + 38 mol % K_2CO_3) at 650°C.

Figure 5. The equivalent circuit representing the corrosion of the base alloy $Fe_{40}Al_{60}$ along with the inter-metallics with 1, 3 and 5 wt. % of Ag in the molten salt (62 mol % Li_2CO_3 + 38 mol % K_2CO_3) at 650°C.

Figure 6a. The cross-sectional SEM image of the $Fe_{40}Al_{60}$ base material after 120 hours of immersion in the molten salt at 650°C.

650°C for 120 hours. After the corrosion test the substrates were cleaned off the corrosion products with acetone and sodium hydroxide according to the ASTM standard G1-03. It was determined the ratio of total weight loss per unit area as a function of exposure time. These values yielded the weight change per unit area of contact of the samples against the test time. Moreover, we calculated the rate of anodic and cathodic corrosion potentials as a function of the metal dissolved in the solution. The weight loss is caused by the anodic oxidation reaction of the metal. Figure 3 shows the weight loss of different materials after being subjected to corrosion tests in the salts, $(LI,K)_2CO_3$, for 120 hours at a temperature of 650°C. This graph shows that the intermetallic materials have a higher weight loss compared to the base material $Fe_{40}Al_{60}$. The weight loss for the $Fe_{40}Al_{60}$ + Ag inter-metallics are about 50 % higher than that of the base material.

The characterization of the electrochemical oxidation of the samples was done in an aqueous solution of the mixture of salts, $(Li,K)_2CO_3$, the temperature of the solution was maintained at 650°± 2°C. We used the electrochemical impedance technique to identify the corrosion mechanisms of the different intermetallic materials. The impedance spectra were recorded at frequency ranges of 100 kHz to 10 mHz with a perturbation of 10 mV applied for all measurements. The electrochemical impedance spectroscopy measurements were carried out using a Solartron SI1260 potentiostat with a frequency analyzer and using the software Z-view and
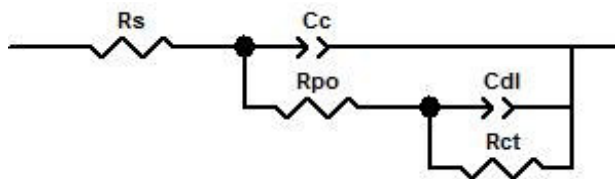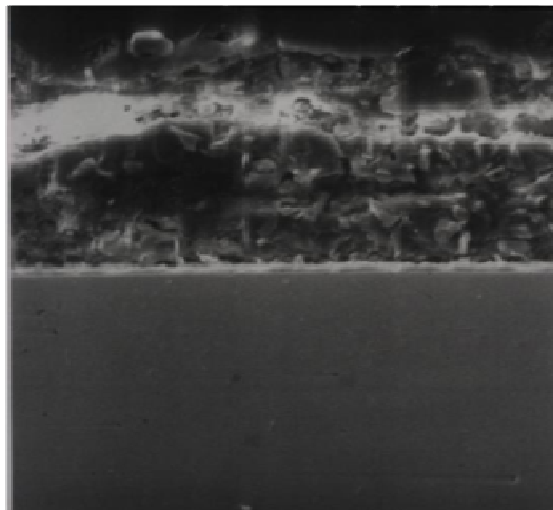
Z-plot. The results obtained from the impedance measurements for the base alloy $Fe_{40}Al_{60}$ and the intermetallic materials $Fe_{40}Al_{60}$ + 1 % Ag, $Fe_{40}Al_{60}$ + 3 % Ag and $Fe_{40}Al_{60}$ + 5 % Ag are presented as the Nyquist plots in figure 4, where there is a real (Z_{re}) and an imaginary (Z_{im}) component for the impedance. The graphs obtained for the base alloy and intermetallic materials exhibit two semicircles, one related to the electrode/electrolyte interface and the other corresponding to the electrode/coating.

The results of the impedance measurements for $Fe_{40}Al_{60}$, $Fe_{40}Al_{60}$ + 1 % Ag, $Fe_{40}Al_{60}$ + 3 % Ag and $Fe_{40}Al_{60}$ + 5 % Ag were modeled to an equivalent circuit which is shown in figure 5, where R_s is the resistance of the electrolyte, C_{dl} the double layer capacitance, R_{ct} the charge transfer resistance, C_c the capacitance of the coating and R_c the coating resistance. Table 3 shows the electrochemical impedance parameters calculated from the impedance

Table 3. The Electrochemical impedance parameters for $Fe_{40}Al_{60}$ and the alloys with the addition of 1, 3, and 5% Ag.

	$Fe_{40}Al_{60}$	$Fe_{40}Al_{60}$ + 1 % Ag	$Fe_{40}Al_{60}$ + 3 % Ag	$Fe_{40}Al_{60}$ + 5 % Ag
Electrolyte resistance (W)	4.86	3.819	5.549	4.873
Charge transfer Resistance (W)	22.58	35.66	1.501	6.239
Polarization Resistance (W)	376.2	759.8	407.2	948.6

Evaluation of the Corrosion Resistance of Fe$_{40}$Al$_{60}$ Intermetallics in Molten Carbonate (Li+K) / *J. New Mat. Electrochem. Systems*
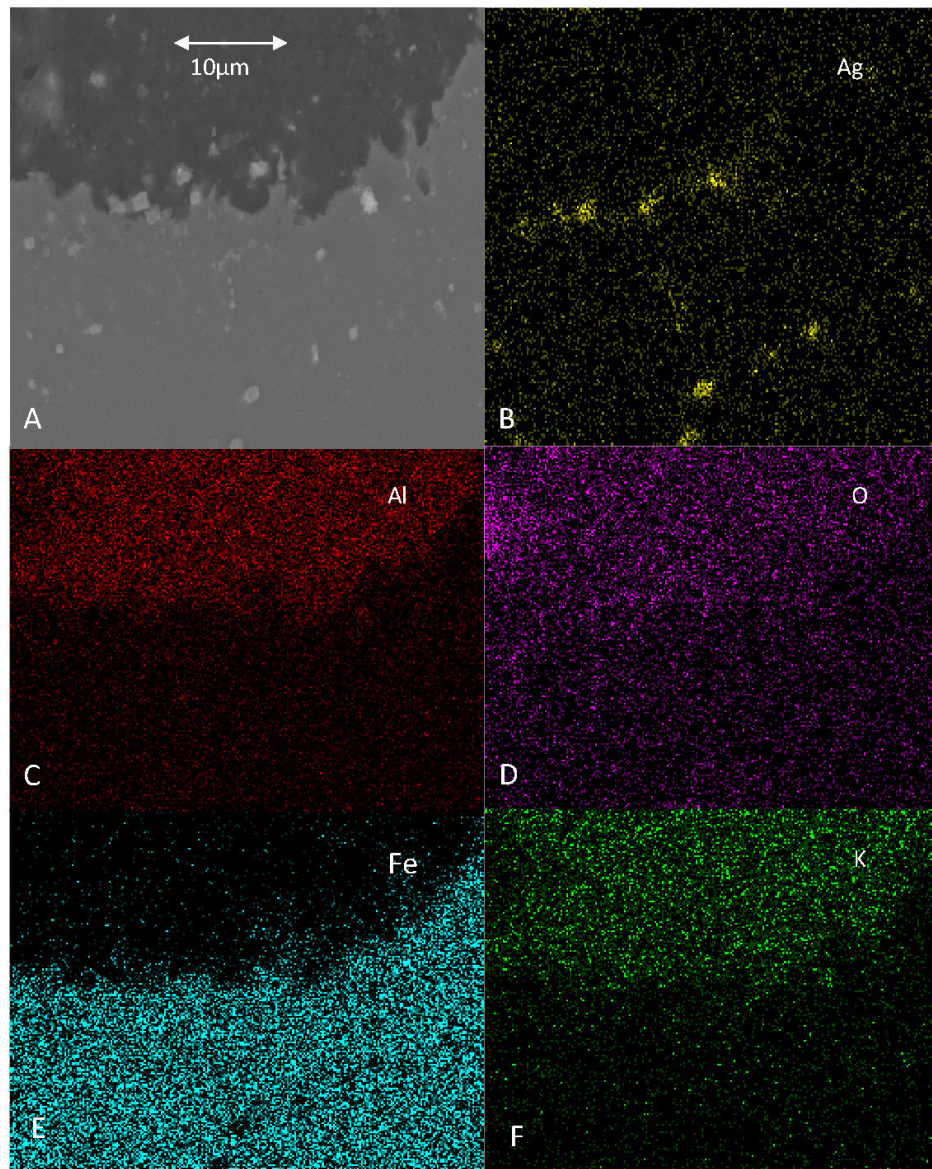
25

Figure 6b. The SEM Photomicrograph of the cross section of the intermetallic alloy Fe$_{40}$Al$_{60}$ + 1 % Ag after 120 hours of immersion in the molten salt at 650°C, showing the distribution of the elements present in the alloy.

analysis. This table shows that the charge transfer resistance for the samples with 3 and 5 % Ag is low compared to the base alloy and hence considered as suitable for application as bipolar plates.

All the samples were analyzed by scanning electron microscopy (SEM). Figure 6 shows the SEM images of the base alloys and the intermetallics before and after the corrosion test. Figure 6a shows the micrograph for the base alloy with typical morphology of the sample cross-section in which one can see the cross-section of the base alloy used in this study. It can be seen that this material has a better protection layer that prevents the advance of corrosion, whereas the inter-metallics (figures 6b, 6c, 6d) containing Ag there is more penetration of the salt onto the surface of the material (zone A).

In the SEM analysis, the elemental mapping technique was used to identify the presence of the elements that constitute each material, along with those formed after being subjected to corrosion testing. Due to the nature of the base material it was necessary to make an elemental chemical mapping to determine the presence of salt-based compounds. Figures 6b-6d show the results for the elemental mapping of the components present in the intermetallic alloys Fe$_{40}$Al$_{60}$ + 1, 3 and 5 % Ag respectively in the molten salt (Li+K) at 650°C. Figure 6b (base alloy + 1 % Ag) shows the distribution of particles of different elements that form the material. The zone A of figure 6 b shows the sample before and after being exposed to the corrosion test, which indicates the deterioration in the sample. The zone B of the figure shows nearly homogeneous distri-
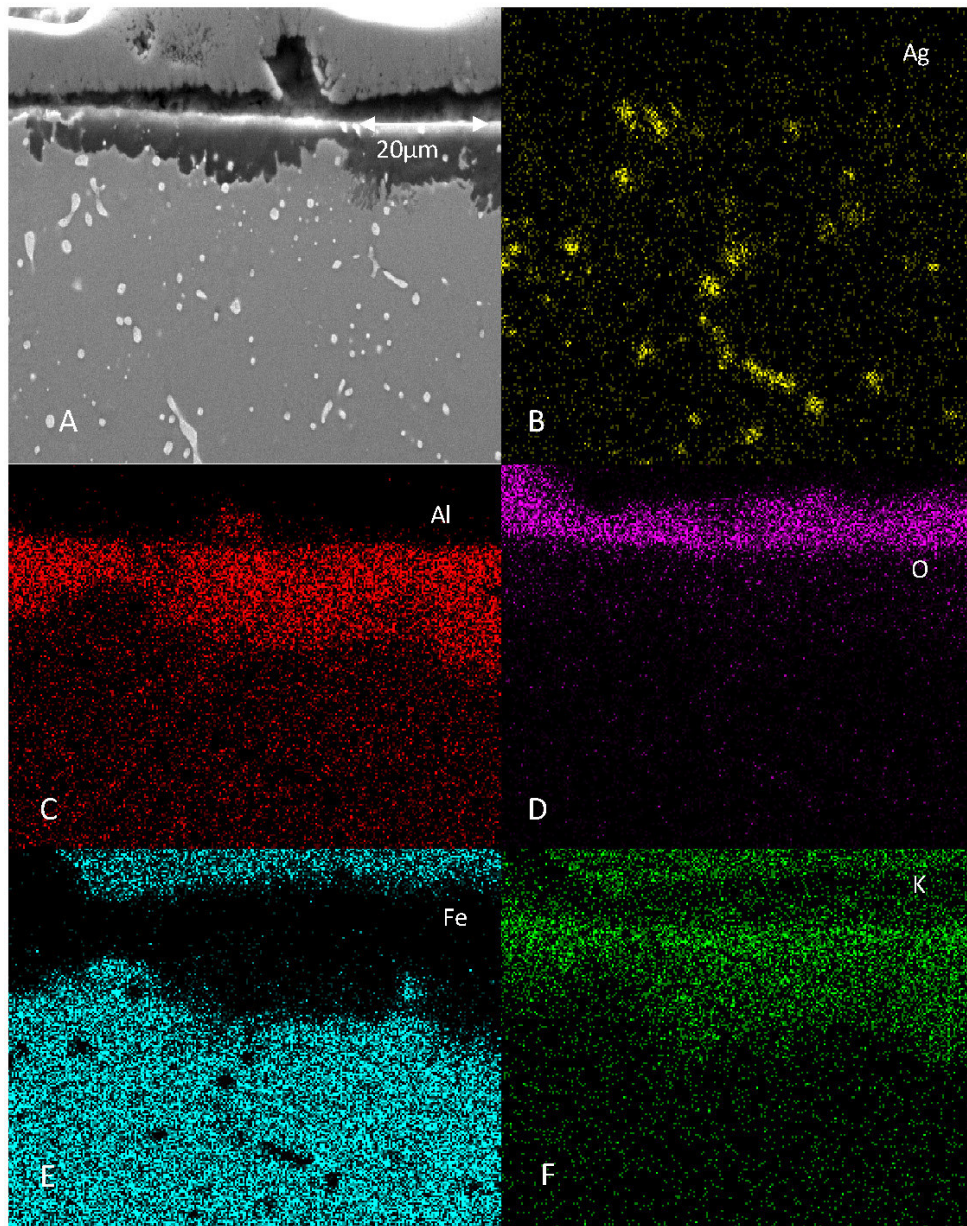
Figure 6c. The SEM Photomicrograph of the cross section of the intermetallic alloy $Fe_{40}Al_{60}$ + 3 % Ag after 120 hours of immersion in the molten salt at 650°C, showing the distribution of the elements present in the alloy.

bution of Ag represented by yellow dots throughout the sample. The zone C of the figure shows the distribution of Al particles in the sample (red dots), with greater presence and homogeneous distribution in the area of corrosion. The zone D of the figure shows the presence of oxygen (pink dots), distributed throughout the sample formed with all metal rusts. The zone E of the figure shows the distribution of Fe particles (blue dots) in the non-corroded simple. The zone F of the figure shows the distribution of the K particles (green dots) in the simple that is homogeneous in the region of the corroded simple.

Figure 6c shows the results for the elemental mapping of the

components present in the intermetallic alloy $Fe_{40}Al_{60}$ + 3 % Ag in the molten salt (Li+K) at 650°C. The zone A of this figure corresponds to the sample before and after being exposed to the corrosion test, which displays the degree of deterioration of the sample. The section B of the figure shows nearly homogeneous distribution of Ag throughout the sample (yellow dots). The area C of the figure shows the distribution of aluminum particles in the sample (red dots), with greater presence and homogeneous distribution in the area of corrosion. The zone D of the figure displays the presence of oxygen (pink dots), distributed throughout the sample formed with metal rusts. The zone E of the figure shows the distribution of Fe
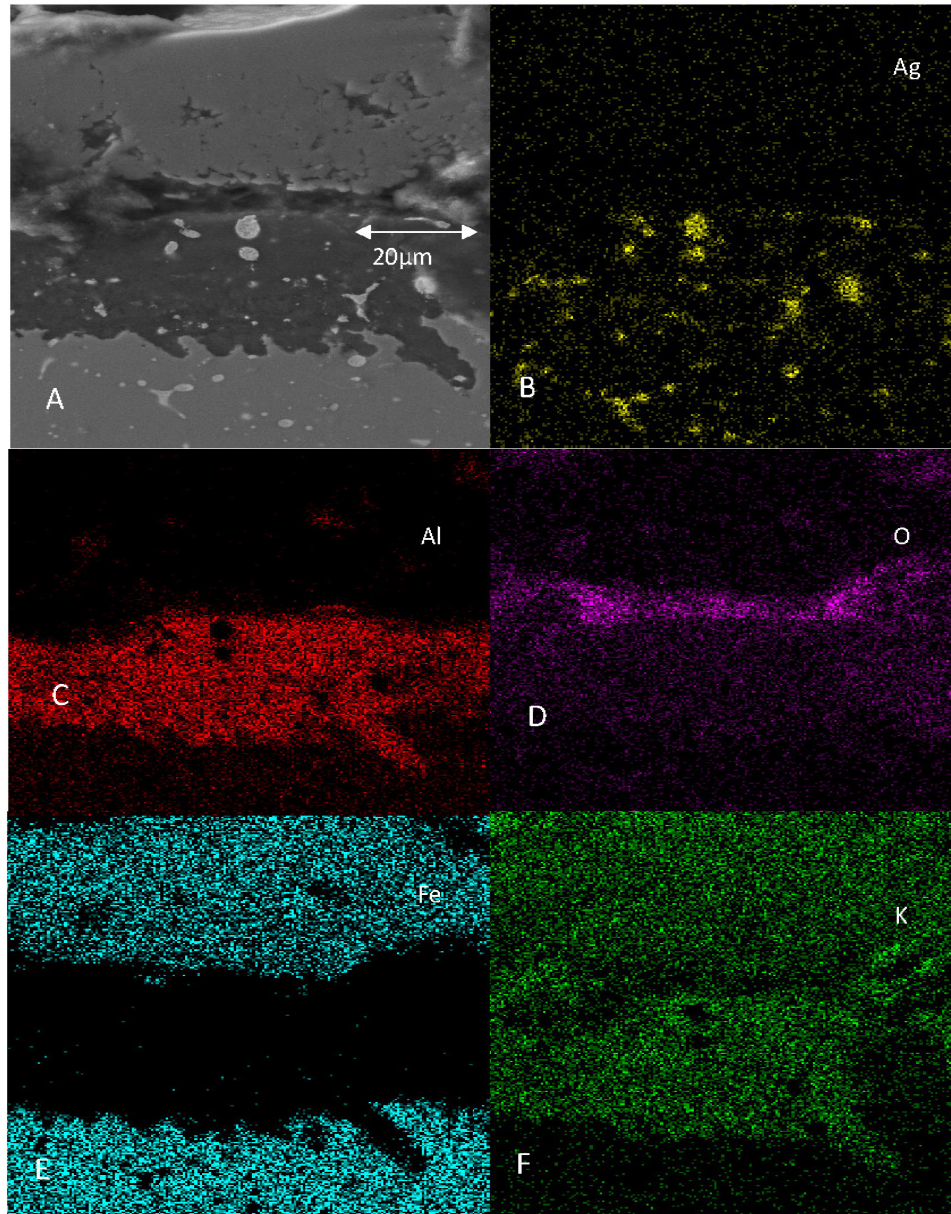
Evaluation of the Corrosion Resistance of Fe$_{40}$Al$_{60}$ Intermetallics in Molten Carbonate (Li+K)
/ J. New Mat. Electrochem. Systems

27

Figure 6d. The SEM Photomicrograph of the cross section of the intermetallic alloy Fe$_{40}$Al$_{60}$ + 5 % Ag after 120 hours of immersion in the molten salt at 650°C, showing the distribution of the elements present in the alloy.

particles (blue dots) in the non-corroded simple. The zone F of the figure shows the distribution of the K particles (green dots) with uniform presence in the area of the corroded sample.

Figure 6d corresponds to the results for the elemental mapping of the components present in the intermetallic alloy Fe$_{40}$Al$_{60}$ + 5 % Ag in the molten salt (Li+K) at 650°C. The zone A of this figure corresponds to the sample before and after being exposed to the corrosion test, which displays the degree of deterioration of the sample. The area B of the figure shows the distribution of Ag throughout the sample (yellow dots). The area C of the figure shows the distribution of aluminum particles in the sample (red dots). The zone D of the figure displays the presence of oxygen (pink dots). The area

E of the figure shows the distribution of Fe particles (blue dots) in the sample. The area F of the figure shows the distribution of the K particles (green dots) in the sample.

The results of the EDS (energy dispersive spectroscopy) analysis of the base material and the intermetallics are shown in figure 7. Figure 7a shows the EDS peaks corresponding to the chemical composition of the materials present on the surface of the simple Fe$_{40}$Al$_{60}$ base material. The components that form the crystalline phase of the material are aluminum in atomic percentage of 19.87 at 0.95 keV peak energy, the atomic percentage for iron is 1.82 at 3.15 keV peak energy and the oxygen atomic percentage is 77.52 in the form of oxide at 0.2 keV peak energy. This technique confirms
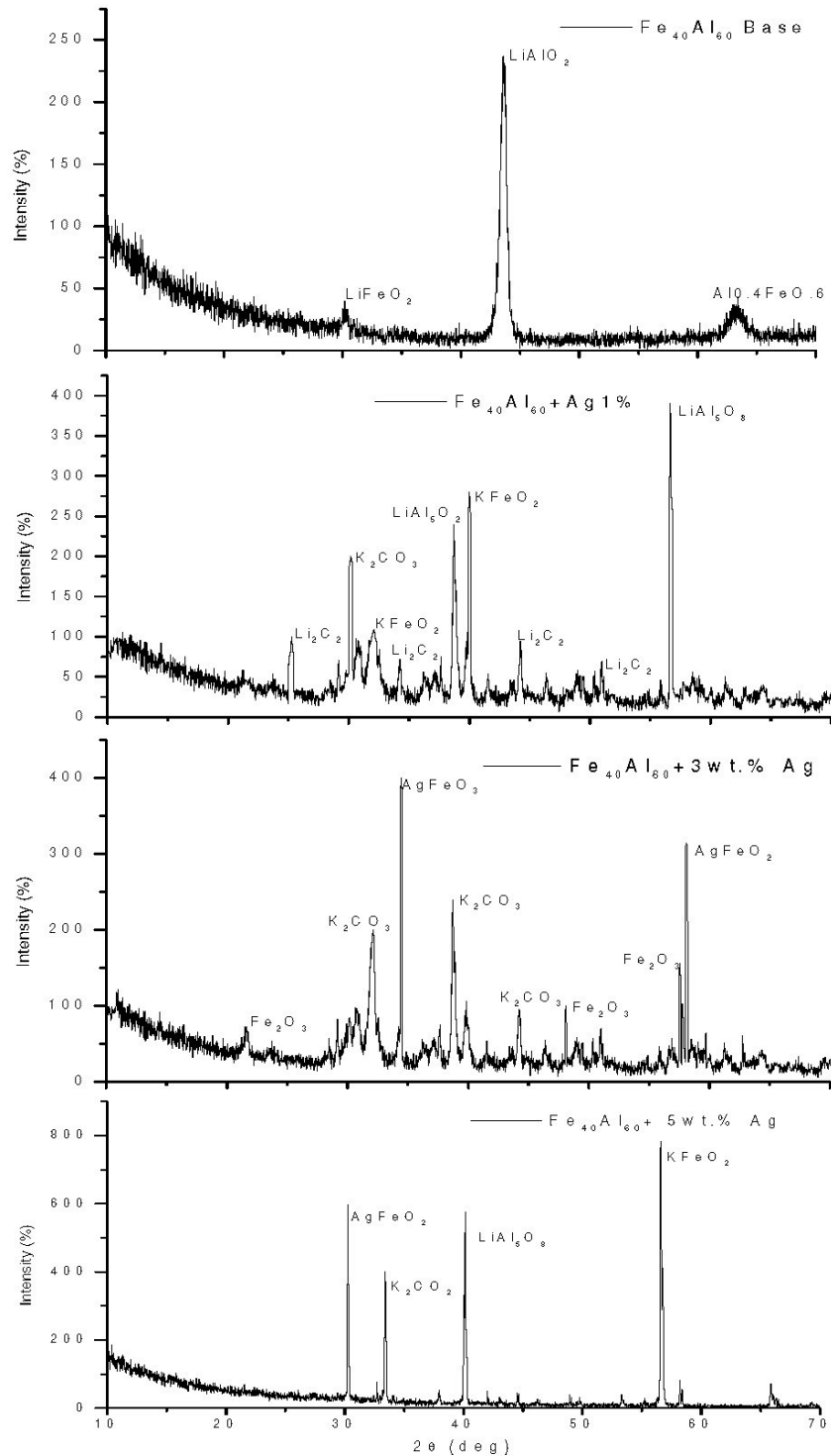
Figure 7. The EDS analysis result for the base alloy $Fe_{40}Al_{60}$ along with the inter-metallics with 1, 3 and 5 wt. % of Ag.

the presence Al anf Fe in the simple. Figure 7b shows the EDS peaks corresponding to the composition of the simple $Fe_{40}Al_{60}$ + 1 % Ag. The atomic percentage of aluminum is 34.93 at the peak energy of 1.55 keV, the atomic percentage of iron is 11.38 at the peak energy of 6.48 keV, and the atomic percentage of silver is 0.5 at the peak energy of 3 keV, confirming the presence of the three elements in the simple. Figure 7c shows the EDS peaks corresponding to the composition of the simple $Fe_{40}Al_{60}$ + 3 % Ag. The

Evaluation of the Corrosion Resistance of Fe$_{40}$Al$_{60}$ Intermetallics in Molten Carbonate (Li+K)
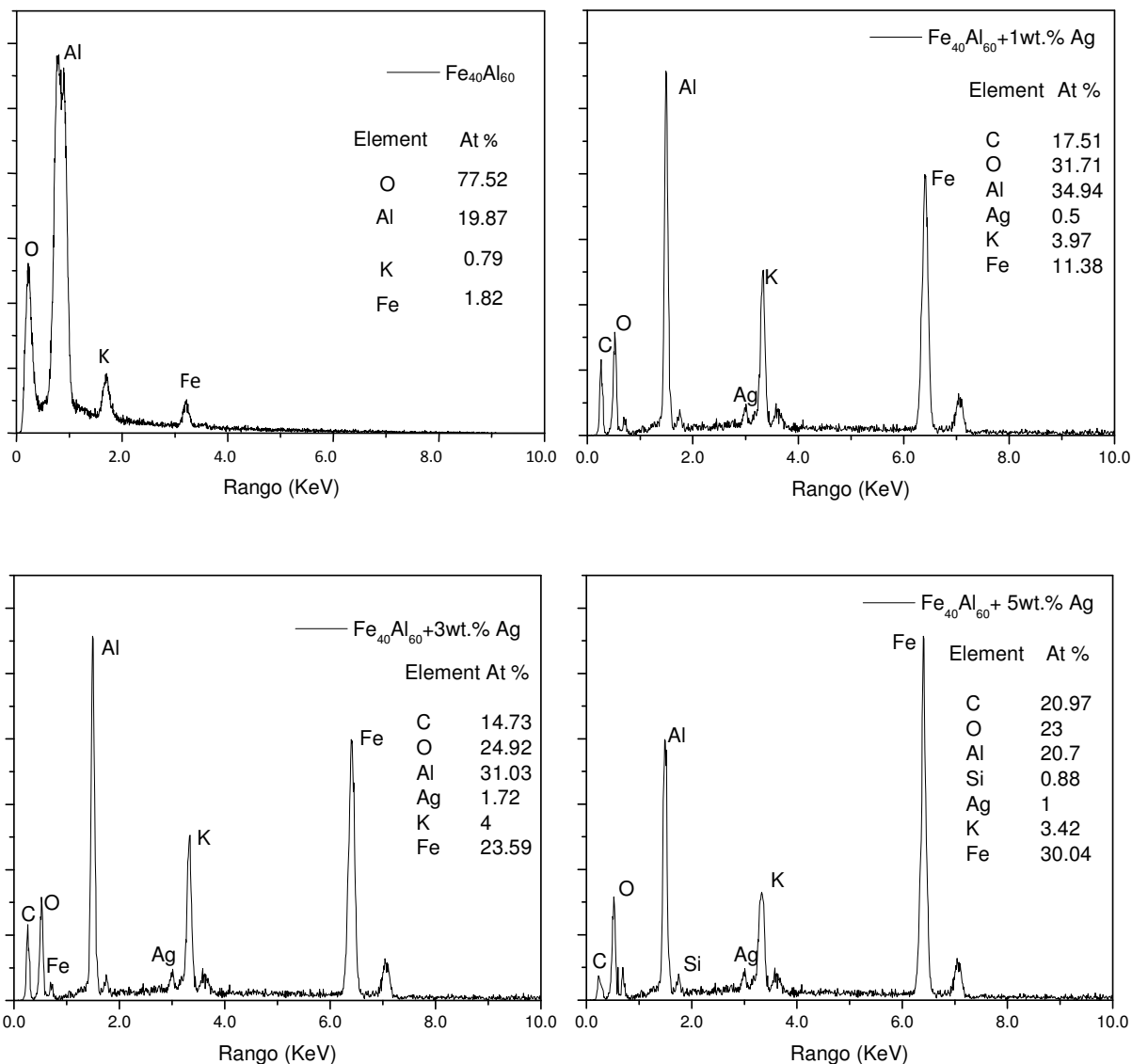*/ J. New Mat. Electrochem. Systems*

29

Figure 8. The XRD patterns for for the base alloy Fe$_{40}$Al$_{60}$ along with the inter-metallics with 1, 3 and 5 wt. % of Ag.

atomic percentage of aluminum is 31.03 at the peak energy of 1.55 keV, the atomic percentage of iron is 23.59 at the peak energy of 6.48 keV and the atomic percentage of silver is 1.72 at the peak energy of 3 keV, confirming the presence of the three elements present in the sample. Figure 7d shows the EDS peaks corresponding to the composition of the simple Fe$_{40}$Al$_{60}$ + 5 % Ag. The atomic percentage of aluminum is 20.7 at the peak energy of 1.55 keV, the atomic percentage of iron is 30.04 at the peak energy of 6.48 keV and the atomic percentage of silver is 1.0 at the peak energy of 3 keV, confirming the presence of the three elements present in the sample.

Figure 8 shows the x-ray diffraction patterns obtained for the different substrates Fe$_{40}$Al$_{60}$ base material, Fe$_{40}$Al$_{60}$ + 1 % Ag, Fe$_{40}$Al$_{60}$ + 3 % Ag and Fe$_{40}$Al$_{60}$ + 5 % Ag. In all the XRD patterns, it is observed the compounds of corrosion product of the interaction

of the alloys with the molten salt (Li,K)$_2$CO$_3$ at the temperature of 650°C. We performed x-ray diffraction of the corrosion products of the samples exposed to the action of high temperature corrosion for 120 hours. Strictly speaking, the molten salt (Li,K)$_2$CO$_3$ is not a corrosion product, where as it is the working salt, the reason why it is present in the diffractograms. The diffraction peaks can also be seen corresponding to the presence of aluminum and oxygen. One can also see the elements of the salts, which were exposed to the substrates (Li, K, C) and as expected the aluminide phase Fe$_{40}$Al$_{60}$ with the oxides of the most important elements of the alloy (LiFeO$_2$ y LiAlO$_2$), figure 8a. Figures 8b, 8c and 8d besides showing the presence of the aluminide phase Fe$_{40}$Al$_{60}$ as in the earlier figure, also show the corrosion products LiFeO$_2$, Fe$_2$O$_3$ and LiAlO$_2$ which have been reported to give some protection against corrosion in molten carbonate mixtures [12.13]. It was not detected the presence

of a protective Al_2O_3, perhaps that was consumed by the $(Li,K)_2CO_3$ salt and was transformed into $LiAlO_2$, something similar was happened to the Fe_2O_3 deposit, which was converted into $LiFeO_2$.

4. CONCLUSIONS

The results obtained in this study indicate that the intermetallic materials based on $Fe_{40}Al_{60}$ with additions of 1, 3 and 5 percent of Ag showed suitable characteristics for their application as bipolar plates in molten carbonate fuel cells. These materials present good corrosion resistance at high temperatures and good electrical conductivity, characteristics that are required for the bipolar plates used in molten carbonate fuel cells. However, more work has to be done in the case of these materials, such as the hydrogen permeability test, studies on variation of Ag amount around 3 % etc. This particular composition showed the best characteristics compared to all other compositions analyzed in this study.

5. ACKNOWLEDGEMENT

REFERENCES

[1] Fuel Cell Handbook, sixth ed., EG&G Technical Services Inc., U.S. Department of Energy, DE-AM26-99FT40575, November, 2002.

[2] P. Capobianco, B. Passalacqua, A. Torazza, Mater. Eng., 10, 25 (1999).

[3] A.J. Appleby, F.R. Foulkes, Fuel Cells Hand Book, Von Nostrand Reimbold, New York, 1989.

[4] K. Joon, J. Power Sources, 71, 12 (1998).

[5] K. Nakagawa, S. Kihara, T. Kobayashi, Proceedings of the 11th International Corrosion Congress, Florence, Italy, 1990.

[6] R.A. Donado, L.G. Marionowski, H.C. Maru, J.R. Selman, J. Electrochem. Soc., 131, 2541 (1984).

[7] C. Yuh, R. Johnson, M. Farouque, H. Maru, J. Power Sources, 56, 1 (1984).

[8] K. Nakagawa, S. Ihara, S. Ito, Corros. Eng., 37, 411 (1988).

[9] R.A. Donado, L.G. Marianowski, H.C. Maru, J.R. Selman, J.Electrochem. Soc., 131, 2535 (1984).

[10] P.F. Tortorelli, P.S. Bishop, in: R.H. Jhones, R.E. Ricker (Eds.), Environmental Effects on Advanced Materials, The Minerals, Metals and Materials Society, Warrendale, 1991, p. 91.

[11] P.F. Tortorelli, K. Natesan, Mater. Sci. Eng., A258, 115 (1998).

[12] M. Salazar, A. ALbiter, F. Rosas, R. Perez, Mater. Sci. Eng., 351ª, 154 (2003).

[13] C. Cuevas-Arteaga, A.J. Uruchurtu-Chavar, J. Porcayo-Calderon, G. Izquierdo-Montalvo, J. González, Corrosion Science, 46, 2663 (2004).

[14] H. Wang, M.P. Brady, G. Teeter, J. Power Sources, 138, 86 (2004).

[15] T.S.N. Sankara Narayanan, Rev. Adv. Mater. Sci., 9, 130 (2005).

[16] D.H. Mesa, S. Amilton, T. Alejandro, T. Andre, Wear, 255, 139 (2003).